Car-Like Ground Vehicle Trajectory Tracking by Using Trajectory Linearization Control

Conference Paper · October 2017
DOI: 10.1115/DSCC2017-5372

2 authors:

Yuanyan Chen
Ohio University
2 PUBLICATIONS **0** CITATIONS
SEE PROFILE

Jim Zhu
Ohio University
135 PUBLICATIONS **1,487** CITATIONS
SEE PROFILE

Proceedings of DSCC 2017
the ASME 2017 Dynamic Systems and Control Conference
October 11-13, 2017, Tyson Coner, Virginia, USA

DSCC2017-5372

CAR-LIKE GROUND VEHICLE TRAJECTORY TRACKING BY USING TRAJECTORY LINEARIZATION CONTROL

Yuanyan Chen
Electric Engineering and Computer Science
Ohio University
Athens, Ohio 45701
Email: yc187911@ohio.edu

J.Jim Zhu*
Electric Engineering and Computer Science
Ohio University
Athens, Ohio 45701
Email: zhuj@ohio.edu

ABSTRACT

This paper focuses on trajectory tracking control for an under-actuated car-like ground vehicle. We consider the 3 degree-of-freedom nonlinear vehicle rigid-body dynamics with nonlinear tire traction force, nonlinear drag forces and actuator dynamics. The control structure employs multi-loop Trajectory Linearization Control (TLC) based on singular perturbation (time-scale separation) theory for exponential stability. The designed controller controls the longitudinal velocity and steering angle simultaneously to follow a feasible guidance trajectory. The paper presents the modeling and design approach with computer simulation results on a scaled-down model car.

INTRODUCTION

The concept of autonomous ground vehicles can be traced back to late 1920 [1]. The first truly autonomous ground vehicle appeared in 1984, with Carnegie Mellon University's Navlab and ALV projects [1]. Early works were focused on improving longitudinal motion, in particular on the traction control (TC) [1], anti-lock braking system (ABS) and adaptive cruise control (ACC) [2]. ACC is for longitudinal trajectory tracking with specified vehicle speed; ABS maintains wheel traction with the road surface in order to prevent uncontrolled skidding by keeping the wheels from locking up during braking; TC helps the vehicle make effective use of the tire traction.

Comparing to mere longitudinal motion control, 3DOF vehicle motion control is more critical and challenging for fully autonomous ground vehicle. First of all, the vehicle rigid-body and tire-force and the various drag force models are highly nonlinear. Secondly, even though the vehicle dynamics may be treated as time invariant, the tracking error dynamics along a time-dependent trajectory are time-varying. Thirdly, the car-like ground vehicles are subject to nonholonomic kinematic constraints, which further necessitates time-varying and non-smooth control laws. Three-DOF motion control is further categorized as path-following and trajectory tracking. Path following only requires the vehicle to follow a specified path without time constraints. Therefore, only vehicle kinematics need to be dealt with by the controller. The trajectory tracking requires the vehicle traverse a prescribed path with a given velocity, which is more challenging than path following, as the vehicle dynamics have to be dealt with as well. In this paper, we focus our work on 3DOF motion control for the non-holonomic ground vehicle trajectory tracking with nonlinear vehicle and force models.

Some of the previous works [3–8] for 3DOF autonomous ground vehicle path following employed model predictive control (MPC) since MPC is known for its capability of systematically taking into account time-varying nonlinearity, control and environment future prediction [8]. MPC is an on-line receding horizon optimal control method. The current control action is obtained by solving the current sampling instant optimal control problem over a finite future time interval. The optimization yields an optimal control sequence, and the first element in the sequence is used as the control for the next sampling time. However there are some practical problems and disadvantages for the MPC: 1) the open-loop optimization cannot guarantee the close-

*Address all correspondence to this author.

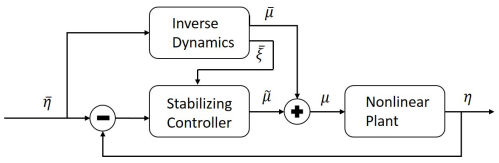

Figure 1: Trajectory Linearization Concept

loop stability [9]; 2) a large number of constraints may render the optimization problem infeasible [10]; 3) computational complexity for high order vehicle dynamics is of $O\left(n_x^2+n_y^2+n_z^2\right)$, where n_x is the number of the states, n_y is the number of the outputs, and n_z is the number of the parameters [7]. One solution for the computational complexity [3] is using linear optimization based on linear approximation of the nonlinear vehicle dynamics which will cause some loss of tracking performance.

Other than MPC, optimal control [11] and sliding mode control [12] have also been used on ground vehicle path following application with low computational cost. But based on our initial search, these two methods are not as widely used as MPC does.

The above mentioned control methods are mostly applied to vehicle path-following. It is noted in [13, 14], trajectory tracking is a nonlinear time varying control problem. Lyapunov based design [15] and Output feedback linearization [16] have been applied in trajectory tracking control for non-holonomic (car-like) robots, but the results reported therein were only verified by simulation or validated on small scale mobile robots for simple trajectories at very low speed.

For better performance, it is desirable to control the translational and rotational motions simultaneously, for which the vehicle dynamics are highly coupled and nonlinear. Thus the controller design is further challenged. Moreover, even though the vehicle plant is time invariant, the trajectory is time varying which will further indicates the tracking error dynamics are time varying. The conventional fixed gain controller is not suitable to solve this kind of problems. The aforementioned MPC is one of the method to deal with the problem. MPC is a time varying controller with anti-causal property, however it is not effective for high-order nonlinear plant due to the computational cost.

In this paper, we propose to use Trajectory Linearization Control (TLC) to deal with the non-holonomic ground vehicle trajectory tracking control problem. TLC consists of an open-loop nominal controller with a closed-loop tracking error regulator, as shown in Figure 1. The nominal controller approximately cancels the plant nonlinearity in the open-loop, thereby reducing the tracking error which facilitates linearization of the nonlinear tracking error dynamics for stabilization. The tracking error dynamics are nonlinear and time varying which are exponentially stabilized using LTV coordinate transformation and PD-eigenvalue assignment. TLC has been applied on a tri-copter drone [17], fixed-wing aircraft [18], omni-direction mobile robot

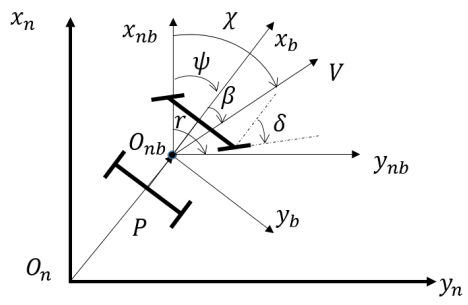

Figure 2: Coordinate Frame

[19] and fixed-wing aircraft loss-of-control [20]. To the best of the author's knowledge, currently TLC has not yet been applied to the car-like ground vehicles. In particular, we modify the previously reported multi-loop trajectory tracking TLC for vehicles without nonholonomic constraints by decoupling the position error in the body-fixed frame rather than in the inertial frame, which enables the controller to handle the nonholonomic constraint on the lateral motion of the vehicle. This modification can also be used on other type of vehicles where the controllability is different along each body axis.

The rest of this paper is organized as follows. After the instruction, 3DOF nonlinear rigid body model for ground vehicles, nonlinear tire force and drag force models, and actuator models are presented in Vehicle Model section. The Trajectory Tracking Control Algorithm Formulation presents technical preliminaries on how the control algorithm is formulated which facilitate the development of the main results. In Trajectory Tracking Controller Design section, 3DOF trajectory tracking controller design is presented in detail. In Simulation Result section, the controller parameters setting and the preliminary simulation results for ground vehicle tracking are presented. The last section is the conclusion.

Vehicle Model

In this section, we define the coordinate frames and the corresponding equations of motion. Three reference frames are employed, a North-East-Down (NED) navigation frame (n-frame), an NED body-carried frame (nb-frame) and a body-fixed frame (b-frame). The n-frame's origin O_b is fixed at a point of interest on the surface of the Earth, which is treated as flat and inertial, with x_n pointing to the north, y_n pointing to the east, and z_n pointing down. The nb-frame is parallel to the n-frame but has the origin O_{nb} at center of the gravity (CG) of the vehicle. For the b-frame, the origin O_b is fixed at the CG of the vehicle, x_b along the longitude of the vehicle pointing forward, y_b pointing to the driver's right side of the vehicle and z_b pointing down. The relationship of the reference frames are shown in Figure 2, where β is the vehicle side-slip angle; δ is the front tire steering

angle; $P = \begin{bmatrix} x_n & y_n \end{bmatrix}^T$ is the vehicle position in the inertial frame; $V = \begin{bmatrix} u & v \end{bmatrix}^T$ is the body frame velocity; ψ is yaw angle; $r = \dot{\psi}$ is the the yaw angular rate.

Rigid-body EOM

For ground vehicle trajectory tracking, we make the following simplifying assumptions: the vehicle is rigid-body; the weight is equally distributed on the four wheels, and the vehicle is driving on level and smooth road. Therefore, pitching and rolling motions are ignored. The current work will focus on combining the longitudinal, lateral motion control with the steering control. Due to the non-holonomic constraint of the car-like ground vehicle, the lateral force can not generate lateral acceleration, so the lateral acceleration is only due to the rotational motion.

Due to the above constraints, the state space equations can be directly simplified from the 6DOF rigid body equation of motion (EOM) to a 3DOF EOM as
Translational Kinematics:

$$\begin{bmatrix} \dot{x}_n \\ \dot{y}_n \end{bmatrix} = \begin{bmatrix} \mathrm{C}_\psi & -\mathrm{S}_\psi \\ \mathrm{S}_\psi & \mathrm{C}_\psi \end{bmatrix} \begin{bmatrix} u \\ v \end{bmatrix} = B_1(\psi) V \tag{1}$$

Here and through out the paper, $\mathrm{S}_\psi = \sin\psi$ and $\mathrm{C}_\psi = \cos\psi$.
Translational Dynamics:

$$\begin{bmatrix} \dot{u} \\ \dot{v} \end{bmatrix} = \begin{bmatrix} 0 & r \\ -r & 0 \end{bmatrix} \begin{bmatrix} u \\ v \end{bmatrix} + \frac{1}{m} \begin{bmatrix} F_x \\ 0 \end{bmatrix} = A_2(r) V + \frac{1}{m} \begin{bmatrix} F_x \\ 0 \end{bmatrix} \tag{2}$$

Rotational Kinematics:

$$\dot{\psi} = r \tag{3}$$

Rotational Dynamics:

$$\dot{r} = \frac{1}{I_{zz}} N_m \tag{4}$$

where $F = \begin{bmatrix} F_x & F_y \end{bmatrix}^T$ is the body frame force with $F_y = 0$ due to the non-holonomic constraint, N_m is the yaw moment, m is the total mass of the vehicles, and I_{zz} is the moment of inertia about the z_b-axis.

Force Model

The total longitudinal force F_x and lateral force F_y are given respectively as

$$\begin{aligned} F_x &= F_{xtf}\cos(\delta) + F_{xtr} - F_{ytf}\sin(\delta) + F_{rr} + F_{aero} + F_B \\ F_y &= F_{xtf}\sin(\delta) + F_{ytf}\cos(\delta) + F_{ytr} + F_{yst} \end{aligned} \tag{5}$$

where $F_{rr} = -C_{rr} mg \mathrm{sgn}(u)$ is the rolling resistance; $F_{aero} = -C_D \frac{\rho}{2} A_F u^2 \mathrm{sgn}(u)$ is the longitudinal aerodynamic drag force and $F_B = \delta_B F_{B,\max}$ is braking force; F_{xt} and F_{yt} are longitudinal and lateral tire force respectively, and F_{yst} is the tire lateral stiction force. Here and throughout the paper the subscripts $_{.f}$ and $_{.r}$ refer to the front and rear axle, respectively.

For wheeled ground vehicles, the propulsion and control forces and the steering moment are effected by the traction forces of the tires. Because of the highly nonlinear behavior, tire force modeling is one of the most significant and difficult part in ground vehicle control.

In this paper, we use the model provided by [21] with some modification. The longitudinal tire force is described as

$$F_{xtr} = F_{xtf} = \frac{1}{2} C_\alpha \alpha(u, \omega_w) \tag{6}$$

where C_α is the 4-wheel total tire stiffness coefficient and α is the longitudinal slip angle which can be defined as

$$\alpha(u, \omega_w) = \begin{cases} \tan^{-1}\dfrac{R_{\text{eff}}\omega_w - u}{u}, \text{ during braking} \\ \tan^{-1}\dfrac{R_{\text{eff}}\omega_w - u}{R_{\text{eff}}\omega_w}, \text{ during acceleration} \end{cases} \tag{7}$$

where R_{eff} and ω_w are the effective radius and angular speed of the wheel, respectively.
The lateral tire force is described as

$$F_{ytf} = \frac{1}{2} C_\beta(\delta - \beta), \;\; F_{ytr} = \frac{1}{2} C_\beta(-\beta) \tag{8}$$

where β defines the tire sideslip angle, δ is vehicle steering angle and C_β is the vehicle total cornering stiffness.

Here we note that, our current work is under no lateral tire skidding assumption, which indicates that the lateral force F_y can not generate lateral displacement, which is a nonholonomic constraint.

The yaw moment is obtained as

$$N_m = \frac{\frac{1}{2}C_\beta l_f - \frac{1}{2}C_\beta l_r}{I_{zz} u} v - \frac{\frac{1}{2}l_f^2 C_\beta + \frac{1}{2}l_r^2 C_\beta}{I_{zz} u} r + \frac{\frac{1}{2}C_\beta l_f}{I_{zz}} \delta \tag{9}$$

where l_f and l_r are the longitudinal distance of the front and rear axle to the center of gravity, here we assume $l_f = l_r$.

Actuator Model

Typical longitudinal traction actuators for automobiles and car-like ground vehicles are either internal combustion engines plus

mechanical brakes, or electrical motors with regenerative braking and mechanical brakes. Steering actuators are typically either hydraulic or electric servos. Here in this paper, we illustrate our design methodology with an armature DC motor as the traction actuator and a servo motor as the steering actuator. But the design can be readily adapted to other types of actuators.

The armature-controlled DC motor can be modeled by the following first-order linear ODE

$$J_m\dot{\omega}_m = -\left(B_m + \frac{K_m^2}{R_a}\right)\omega_m + \frac{K_m}{R_a}E_m - NR_{\text{eff}}F_{xL} \tag{10}$$

where F_{x_L} is longitudinal load force; R_a is the armature resistance; J_m is the effective moment of inertia of the drive train about the motor shaft, and B_m is the effective torsional viscous friction coefficient of the drive train about the motor shaft; K_m is motor electro-mechanical constant; R_{eff} is effective radius of the tire.

Dynamics of the steering servo can be modeled with a transfer function $G(s) = \frac{\omega_{ns}}{s+\omega_{ns}}$ to represent its dynamics, where ω_{ns} is the bandwidth of the servo motor.

Trajectory Tracking Control Algorithm Formulation

First, we will formulate the nonlinear trajectory tracking problem as a stabilization problem in the tracking error coordinate, which will reveal that the tracking error dynamics are time-varying for time-varying nominal trajectories, even if the vehicle dynamics are time-invariant. The TLC architecture is then introduced as a natural solution to this problem formulation for trajectory tracking.

Consider the nonlinear plant

$$\dot{\xi}(t) = f(\xi(t),\mu(t)),\ \ \eta(t) = h(\xi(t),\mu(t)) \tag{11}$$

where $\xi(t) \in \mathbb{R}^n, \mu(t) \in \mathbb{R}^l, \eta(t) \in \mathbb{R}^m$ are the state, input and output respectively. The mappings $h(\cdot) : \mathbb{R}^n \times \mathbb{R}^l \to \mathbb{R}^n$ and $f(\cdot) : \mathbb{R}^n \times \mathbb{R}^l \to \mathbb{R}^n$ are bounded with uniformly bounded and continuous Jacobians. Let $\bar{\xi}(t), \bar{\mu}(t), \bar{\eta}(t)$ be the nominal state, nominal input and nominal output trajectory such that

$$\dot{\bar{\xi}}(t) = f\left(\bar{\xi}(t),\bar{\mu}(t)\right),\ \ \bar{\eta}(t) = h\left(\bar{\xi}(t),\bar{\mu}(t)\right) \tag{12}$$

and define the respective tracking errors and error control as

$$\tilde{\xi}(t) = \xi(t) - \bar{\xi}(t),\ \tilde{\eta}(t) = \eta(t) - \bar{\eta}(t),\ \tilde{\mu}(t) = \mu(t) - \bar{\mu}(t) \tag{13}$$

Then the tracking error dynamics can be written as

$$\begin{aligned}\dot{\tilde{\xi}} &= f\left(\bar{\xi}(t) + \tilde{\xi}, \bar{\mu}(t) + \tilde{\mu}\right) - f\left(\bar{\xi}(t), \bar{\mu}(t)\right) \\ &= F\left(\tilde{\xi}, \tilde{\mu}, \bar{\xi}(t), \bar{\mu}(t)\right) \\ \tilde{\eta} &= h\left(\bar{\xi}(t) + \tilde{\xi}, \bar{\mu}(t) + \tilde{\mu}\right) - h\left(\bar{\xi}(t), \bar{\mu}(t)\right) \\ &= H\left(\tilde{\xi}, \tilde{\mu}, \bar{\xi}(t), \bar{\mu}(t)\right)\end{aligned} \tag{14}$$

where $\bar{\xi}(t), \bar{u}(t)$ can be treated as known time-varying parameters. The nominal control input $\bar{\mu}(t)$ and nominal state $\bar{\xi}(t)$ can be obtained by pseudoinversion of the plant (11).

The tracking error dynamics (14) are nonlinear time-varying, which can be linearized along the nominal trajectories to obtain

$$\dot{\mathbf{x}} = A(t)\mathbf{x} + B(t)\mathbf{u},\ \ \mathbf{y} = C(t)\mathbf{x} + D(t)\mathbf{u} \tag{15}$$

where $\mathbf{x} \approx \tilde{\xi}, \mathbf{y} \approx \tilde{\eta}$ and $\mathbf{u} \approx \tilde{\mu}$, and

$$\begin{aligned}A &= \frac{\partial}{\partial\tilde{\xi}} f(\xi,\mu)\,|_{\bar{\xi},\bar{\mu}} = \frac{\partial}{\partial\tilde{\xi}} F\left(\tilde{\xi},\tilde{\mu},\bar{\xi},\bar{\mu}\right)|_{\tilde{\xi},\tilde{\mu}=0} \\ B &= \frac{\partial}{\partial\tilde{\mu}} f(\xi,\mu)\,|_{\bar{\xi},\bar{\mu}} = \frac{\partial}{\partial\tilde{\mu}} F\left(\tilde{\xi},\tilde{\mu},\bar{\xi},\bar{\mu}\right)|_{\tilde{\xi},\tilde{\mu}=0} \\ C &= \frac{\partial}{\partial\tilde{\xi}} h(\xi,\mu)\,|_{\bar{\xi},\bar{\mu}} = \frac{\partial}{\partial\tilde{\xi}} H\left(\tilde{\xi},\tilde{\mu},\bar{\xi},\bar{\mu}\right)|_{\tilde{\xi},\tilde{\mu}=0} \\ D &= \frac{\partial}{\partial\tilde{\mu}} h(\xi,\mu)\,|_{\bar{\xi},\bar{\mu}} = \frac{\partial}{\partial\tilde{\mu}} H\left(\tilde{\xi},\tilde{\mu},\bar{\xi},\bar{\mu}\right)|_{\tilde{\xi},\tilde{\mu}=0}\end{aligned} \tag{16}$$

The linearized tracking error dynamics (15) can be stabilized by applying the linear time-varying control law $\mathbf{u} = K(t)\mathbf{x}$. The TLC combines nonlinear inversion and the linear time-varying feedback stabilization. Since the stabilization is exponential, it provides robust stability in the presence of regular and singular perturbations.

Trajectory Tracking Controller Design

The TLC control algorithm presented in the previous section is used next to design a 3DOF controller for the non-holonomic ground vehicle. The block diagram of the overall control system is shown in Figure 3. A novel feature of our design method is that the vehicle model is divided as the rigid-body model, the force model and the actuator model, and each sub-model is handled separately. The controller consists of two parts, guidance controller on the left and steering controller on the right in Figure 3. The overall closed-loop system consists of 4 loops.

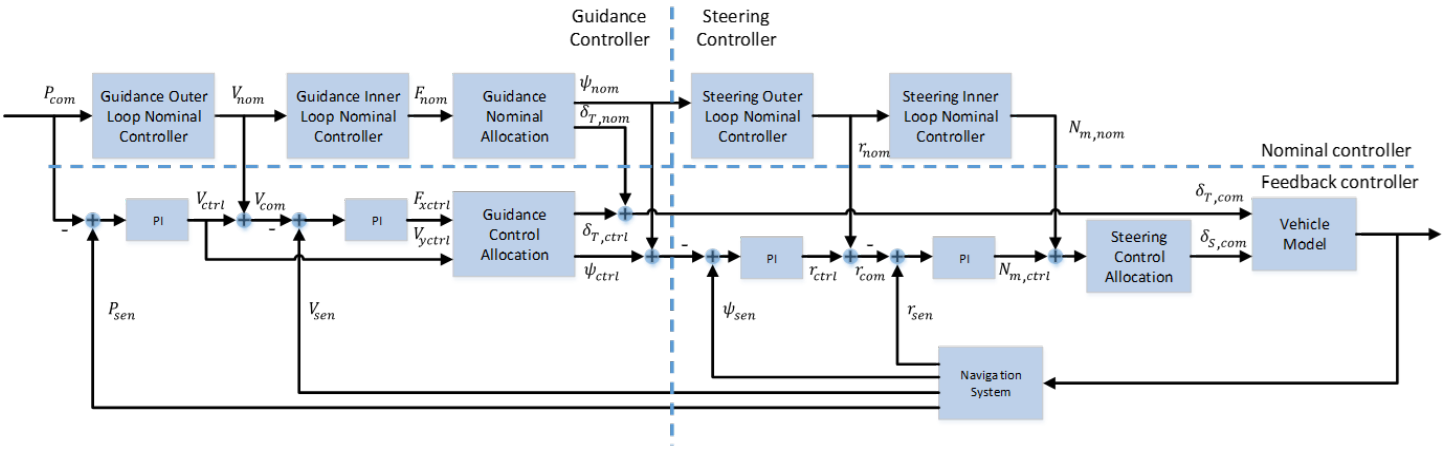

Figure 3: 3DOF Trajectory Linearization Controller Block Diagram

Each loop has the complete TLC structure as shown in Figure 1. The open-loop nominal controllers on the top of Figure 3 use dynamic pseudo-inverse of the corresponding EOMs to generate the nominal control signals and nominal states, and the feedback controllers at the bottom of Figure 3 uses Proportional-Integral (PI) control laws to exponentially stabilize the tracking errors. Here and throughout the paper, $*_{sim}$ represents the simulated vehicle state variables, $*_{sen}$ is the simulated vehicle states passed through navigation sensors. $*_{nom}$ is the nominal signal, $*_{ctrl}$ is PI controller output, $*_{err}$ is the tracking error, and $*_{com}$ is the command signal, which is the sum of the nominal signal and the controller signal.

Guidance Outer Loop

The guidance outer loop takes position command and position measurement to calculate the velocity command for the inner loop. The nominal body frame velocity can be obtained by inverting Eq (1) as

$$V_{nom} = B_1^{-1}(\psi_{nom})\,\dot{P}_{nom} \tag{17}$$

where $B_1(\psi_{nom})$ is the matrix in Eq (1) with ψ replaced by its nominal value ψ_{nom}. Here ψ_{nom} is defined in the Guidance Nominal Allocation sub-section and $\dot{P}_{nom}$ is obtained from position command by a pseudo-differentiator of the form

$$G_{\text{diff}}(s) = \frac{\omega_{n,\text{diff}}^2 s}{s^2 + 2\zeta_{\text{diff}}\omega_{n,\text{diff}} s + \omega_{n,\text{diff}}^2} \tag{18}$$

Define the position tracking error $P_{err} = P_{sen} - P_{nom}$. Due to the non-holonomic constraint on the lateral motion of a car-like ground vehicle, we will decouple the tracking error dynamics

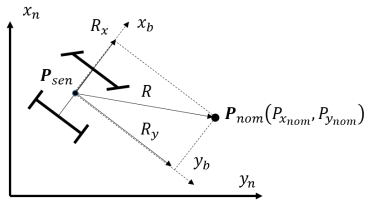

Figure 4: Error Coordinate Frame

in the b-frame, rather than in the n-frame as it has been done in all previously published TLC design for holonomic vehicles. Define down range vector $R_b = -B_1^{-1}(\psi_{nom})\,P_{err}$, which is the projection of the $-P_{err}$ on the body frame as shown in Figure 4.

The linearized error dynamics is then given by

$$\dot{R}_b = \begin{bmatrix} 0 & r_{nom} \\ -r_{nom} & 0 \end{bmatrix} R_b + V_{ctrl} \tag{19}$$

The PI control law is given as

$$V_{ctrl} = -K_{P1}R_b - K_{I1}\int_0^t R_b(\tau)\,d\tau \tag{20}$$

where the PI gain matrices are designed as

$$\begin{aligned} K_{P1} &= \begin{bmatrix} 0 & r_{nom} \\ -r_{nom} & 0 \end{bmatrix} - A_{1.1} = \begin{bmatrix} a_{111} & r_{nom} \\ -r_{nom} & a_{121} \end{bmatrix} \\ K_{I1} &= -A_{1.2} = \begin{bmatrix} a_{112} & 0 \\ 0 & a_{122} \end{bmatrix} \end{aligned} \tag{21}$$

where $A_{i.k} = \text{diag}\left[-a_{i1k}\ -a_{i2k}\right], i = 1,2,3,4$ and $k = 1,2$ are time-varying controller parameters which synthesized from the

desired closed-loop dynamic.

$$a_{ij1} = 2\zeta_{ij}\omega_{n,ij}, \;\; a_{ij2} = \omega_{n,ij}^2 \tag{22}$$

where $\omega_{n,ij}$ are the desired natural frequency, and $\zeta_i j$ are the desired constant damping ratio of the desired dynamics; $j = 1,2$ for the x and y channel, and $i = 1,2$ for the two guidance loops. The output of the guidance outer loop combines the nominal controller output and feedback controller output $V_{com} = V_{nom} + V_{ctrl}$.

Guidance Inner Loop

The guidance inner loop takes velocity command V_{com} from the the guidance outer loop and velocity measurement V_{sen} to calculate the force command for the guidance loop control allocation.

The nominal force is calculated from the translational dynamics Eq (2)

$$F_{nom} = m\left[\dot{V}_{nom} - A_2\left(r_{nom}\right)V_{nom}\right] \tag{23}$$

where $\dot{V}_{nom} = \left[\dot{u}_{nom} \; \dot{v}_{nom}\right]^T$ is obtained by passing the V_{nom} through a pseudo-differentiator Eq (18).

Define the velocity tracking error as $V_{err} = V_{sen} - V_{com}$. The linearized error dynamics of the body velocity is given as:

$$\dot{V}_{err} = A_2\left(r_{nom}\right)V_{err} + \frac{1}{m}F_{ctrl} \tag{24}$$

where $A_2(\cdot)$ is the matrix in Eq (2). The guidance inner loop PI control law is defined as

$$F_{ctrl} = -K_{P2}V_{err} - K_{I2}\int_0^t V_{err}(\tau)d\tau \tag{25}$$

The body velocity PI parameters are given as

$$\begin{aligned} K_{P2} &= m\left[A_2\left(r_{nom}\right) - A_{2.1}\right] = m\begin{bmatrix} a_{211} & r_{nom} \\ -r_{nom} & a_{221}\end{bmatrix} \\ K_{I2} &= -mA_{2.2} = m\begin{bmatrix} a_{212} & 0 \\ 0 & a_{222}\end{bmatrix} \end{aligned} \tag{26}$$

As we mentioned before, car-like ground vehicle is nonholonomic, so in the b-frame the lateral force cannot generate lateral displacement. Here we only use x-channel of F_{nom} and F_{ctrl} to deal with throttle control. The lateral position error will be corrected by the yaw angle ψ, which will be stated in the next subsection.

Guidance Allocation

The guidance allocation unit is used to calculate the throttle command $\delta_{T,com}$ and the yaw command ψ_{com}. Under the rigid body and level ground assumptions, the rotational motion is only dependent on yaw angle ψ. Thus, the roll angle ϕ and pitch angle θ can either be constrained to zero or treated as disturbances. The force F_x is allocated to the throttle control, which in this paper is the applied voltage of the DC motor.

For a DC motor drive car, $\delta_T = E_m$. The applied motor voltage is obtained by inverting Eq (10)

$$\begin{aligned} \delta_{T,com} = E_m = \frac{J_m R_a}{K_m}\dot{\omega}_{m_{nom}} + \left(\frac{B_m R_a}{K_m} + K_m\right)\omega_{m_{nom}} \\ + \frac{R_{\text{eff}} R_a}{K_m}F_{x_{com}} \end{aligned} \tag{27}$$

where $\omega_{m_{nom}}$ is obtained from the nominal angular speed of the wheel $\omega_{w_{nom}}$, which is calculated by inverting Eq (6) with nonlinear tire force model (7); $\dot{\omega}_{m_{nom}}$ is obtained by passing $\omega_{m_{nom}}$ through a pseudo-differentiator.

From Figure 2, $\psi = \chi - \beta$, where β is vehicle sideslip angle. The nominal course angle χ_{nom} is defined as $\chi_{nom} = \tan^{-1}\frac{\dot{x}_{n,nom}}{\dot{y}_{n,nom}}$. Since β makes the dynamic inverse unstable, it is excluded from the nominal dynamic inverse. So let $\beta_{nom} = 0$, then $\psi_{nom} = \chi_{nom}$. We will let the feedback controller deal with β. Define

$$\psi_{ctrl} = \beta_{ctrl} = \tan^{-1}\frac{v_{ctrl}}{u_{nom}} \tag{28}$$

where v_{ctrl} is the second channel of V_{ctrl} from the guidance outer loop. So $\psi_{com} = \psi_{nom} + \psi_{ctrl}$.

Steering Outer Loop

The outer loop of the Steering controller takes yaw command ψ_{com} from the guidance allocation and the yaw measurement ψ_{sen} to calculate the body angular rate command for the inner loop. By inverting Eq (3)

$$r_{nom} = \dot{\psi}_{nom} \tag{29}$$

where $\dot{\psi}_{nom}$ is obtained by passing ψ_{nom} through the pseudo-differentiator (11). The tracking error control law for this loop is

$$r_{ctrl} = -K_{P3}\psi_{err} - K_{I3}\int_0^t \psi_{err}(\tau)dt \tag{30}$$

where $\psi_{err} = \psi_{sen} - \psi_{nom}$ is the yaw tracking error. The control gains are given as

$$K_{P3} = a_{331}, \;\; K_{I3} = a_{332} \tag{31}$$

Figure 5: Traxxas Electric Ground Vehicle

The output of Steering outer loop is $r_{com} = r_{nom} + r_{ctrl}$.

Steering Inner Loop

The Steering inner loop takes body yaw rate command and yaw rate measurement to calculate the torque command for the Steering control allocation.

By inverting Eq (4), the nominal body torque is given as

$$N_{m_{nom}} = I_{zz}\dot{r}_{nom} \tag{32}$$

where $\dot{r}_{nom}$ is obtained by passing r_{nom} through a pseudo-differentiator.

The PI control law for the inner loop is

$$N_{m_{ctrl}} = -K_{P4}r_{err} - K_{I4}\int_0^t r_{err}(\tau)dt \tag{33}$$

where $r_{err} = r_{sen} - r_{nom}$ is the body angular rate tracking error and the control gains are given as

$$K_{P4} = I_{zz}a_{431}, \;\; K_{I4} = I_{zz}a_{432} \tag{34}$$

The output of the Steering inner loop is $N_{m_{com}} = N_{m_{nom}} + N_{m_{ctrl}}$.

Steering Allocation

The steering allocation unit is used to allocate the moment command to steering angle and further calculate the steering actuator command $\delta_{S,com}$. The steering angle command $\delta_{S,com}$ is obtained by inverting Eq (10)

$$\delta_{S,com} = \left(N_{m_{com}} + \frac{C_\beta(l_f^2 + l_r^2)r_{nom}}{u_{nom}}\right)\cdot\frac{2}{C_\beta l_f} \tag{35}$$

Simulation and Results

To focus on the motion control issues, and to facilitate validation of the controller design, we have designed a 3DOF trajectory tracking controller for a DC motor driven car with regenerating braking and servo motor driven steering. The controller for 3DOF car takes the position trajectory as command and calculates the corresponding voltages for the motor and the steering servo.

Table 1: Vehicle Modeling Parameters for Traxxas RC vehicle

R_{eff}	Effective wheel radius	0.0725	m
L	Length of the longitudinal axle	0.7	m
w	Width of the vehicle track	0.35	m
m	Total mass	4.76	kg
I_{zz}	Moment of inertia about z-axis	0.0687	$\text{kg}\cdot\text{m}^2$
C_α	Total longitudinal tire stiffness	400	$\frac{\text{N}}{\text{rad}}$
C_{rr}	Total tire rolling resistance	0.02	
C_β	Total cornering stiffness	150	$\frac{\text{N}}{\text{rad}}$
J_m	Motor moment of inertia	$5.4e^{-5}$	$\text{kg}\cdot\text{m}^2$
B_m	Motor viscous friction constant	$0.5e^{-5}$	$\frac{\text{Nm}}{\text{rad·s}}$
K_m	Motor KM constant	$5.15e^{-3}$	$\text{N}\cdot\text{m/A}$
R_a	Total armature resistance	0.2	Ω
N	Gear ratio	$\frac{1}{20}$	

In our current work, the 3DOF controller is implemented and tested in MATLAB/SIMULINK. The vehicle rigid-body model is built based on (1) $\sim$ (4); the tire force model is based on (5) $\sim$ (7), along with various nonlinear drage forces and actuator models as given in (9) and (10). The system parameters in Table 1 are based on the Traxxas RC model car as shown in Figure 5. The controller is implemented according to the design in the previous section and the controller coefficients are given in Table 2. We consider the scenarios where the objective is to follow a desired trajectory as close as possible and keep the desired velocity as well. The following saturation requirements have been imposed on the controller: $|\delta| \leq 30$ and $|u| \leq 7$ m/s.

Simulation results are given in Figures 6 $\sim$ 15. Figure 6 shows the 2D view of the trajectory command and the vehicle position along the ground in the n-frame. The command signal is a feasible trajectory for which the steering and speed saturation constraints are satisfied. Figure 7 shows the position tracking performance for each state variable and the corresponding tracking errors in the n-frame and b-frame are shown in Figure 8 and Figure 9, respectively. The position error P_{err} in n-frame is defined in Figure 4, which is the derivation of the vehicle's current position from the nominal position. The b-frame error is the projection of P_{err} onto the b-frame. From Figure 9, we notice that the longitudinal tracking error quickly converges to 0 after the vehicle achieves the steady state. The maximum lat-

Table 2: Three-DOF Motion Controller Coefficients

	Guidance Outer Loop	Guidance Inner Loop	Steering Outer Loop	Steering Inner Loop
Nominal Controller				
ζ	1.4	1.4	1.4	1.4
ω_n	9	9	14	14
Feedback Controller				
ζ	$\begin{bmatrix}0.7 & 2.1\end{bmatrix}$	$\begin{bmatrix}0.7 & 1.4^*\end{bmatrix}$	0.7	0.7
ω_n	$\begin{bmatrix}3 & 0.9\end{bmatrix}$	$\begin{bmatrix}16 & 4^*\end{bmatrix}$	5	17

**The second channel of guidance inner loop is not used due to non-holonomic constraint*

eral tracking error R_{by} is about 0.09m, which is approximately 26% vehicle track width at about 21s and 61s. These are due to the large turning rate and angular acceleration when the path has a sharp turn, as shown in Figure 14. In general, higher speed will cause larger lateral tracking errors at turns. Figure 10 could explain this phenomenon. The vehicle driving at 6 m/s would bring the maximum lateral tracking error up to 0.3 m, 86% track width; while $u = 2$ m/s reduces the maximum tracking error to 0.01 m, 3% track width. The current trajectory requires the 1/6-scale vehicle driving with $u = 4$ m/s, which is about 54 mph for a full-size car. Figure 11 shows the velocity tracking in the b-frame, and the corresponding tracking error is shown in Figure 12. The directional tracking performance is shown in Figure 13 and the corresponding tracking error is shown in the bottom half. The difference between ψ_{com} and ψ_{nom} is the vehicle side slip angle β. The angular rate tracking is presented in Figure 14. Figure 15 is the actuator signals for the DC motor and electrical servo which are smooth and well within the saturation limits.

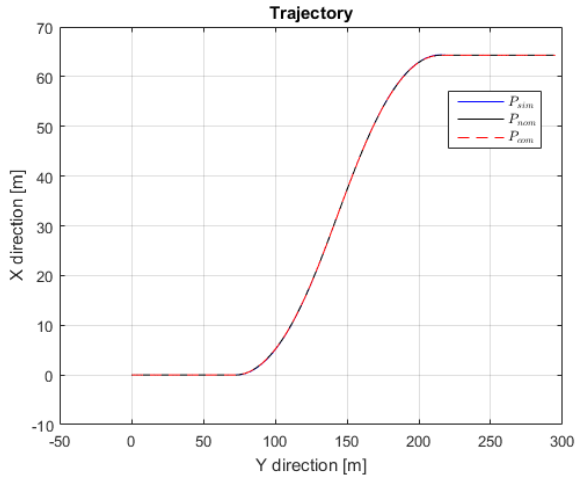

Figure 6: Position Trajectory Tracking Performance in n-frame

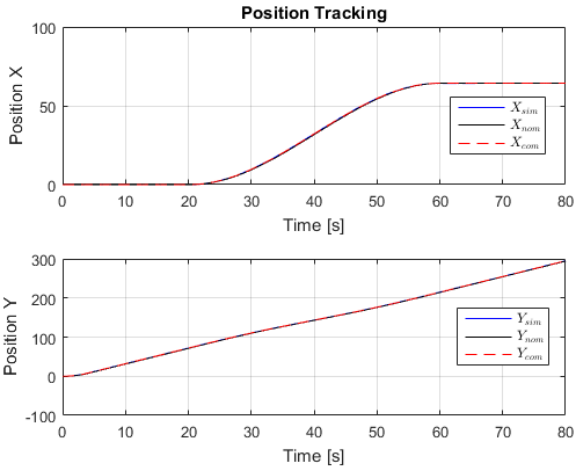

Figure 7: Position Tracking

Summary and Conclusion

In this paper, we have presented a 3DOF trajectory tracking controller design for nonlinear, non-holonomic car-like ground vehicle using TLC. The simulation results show that the vehicle can track a feasible trajectory with good performance. This could have been the first TLC controller for non-holonomic vehicle trajectory tracking, and it provides an effective alternative to MPC and other car controllers. The current controller is being implemented on the Traxxas RC model car for validation. In the future, we will further improve the controller by taking into consideration of the sensor errors, dynamics and noise, the deformable connection between the vehicle body and wheels, and the rolling and pitching motions, tire skidding as well as vehicle stability.

REFERENCES

[1] Wallace, Richard, et al. "First Results in Robot Road-Following." IJCAI. 1985.

[2] Wang, Junmin, and R. Rajamani. "The impact of adaptive cruise control systems on highway safety and traffic flow." Proceedings of the Institution of Mechanical Engineers, Part D: Journal of Automobile Engineering 218.2 (2004): 111-130.

[3] Falcone, Paolo, et al. "Predictive active steering control for autonomous vehicle systems." IEEE Trans on control systems technology 15.3 (2007): 566-580.

[4] Falcone, Paolo, et al. "A hierarchical model predictive control framework for autonomous ground vehicles." American Control Conference. IEEE, 2008.

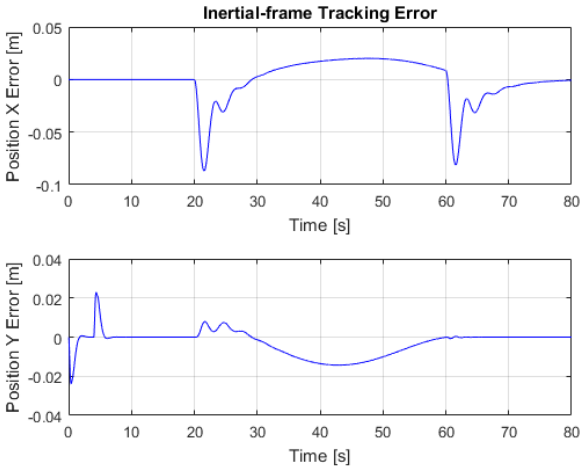

Figure 8: Position Tracking Error in n-frame

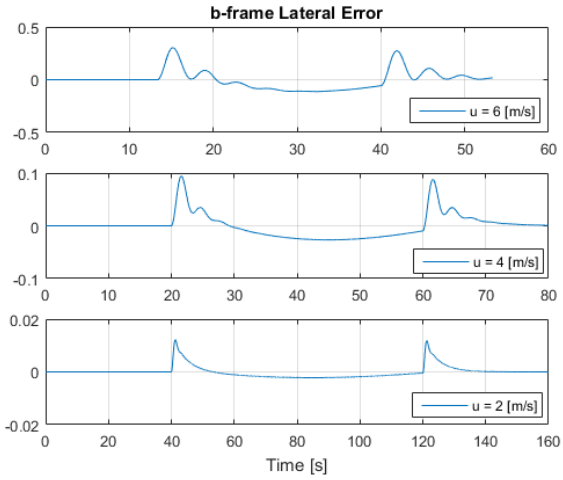

Figure 10: Lateral Error at Different Speeds

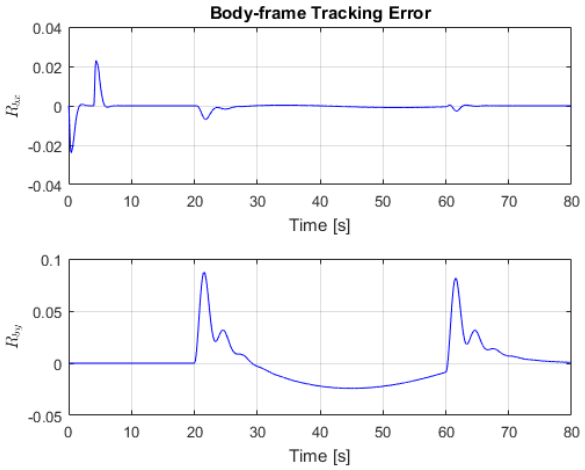

Figure 9: Position Tracking Error in b-frame

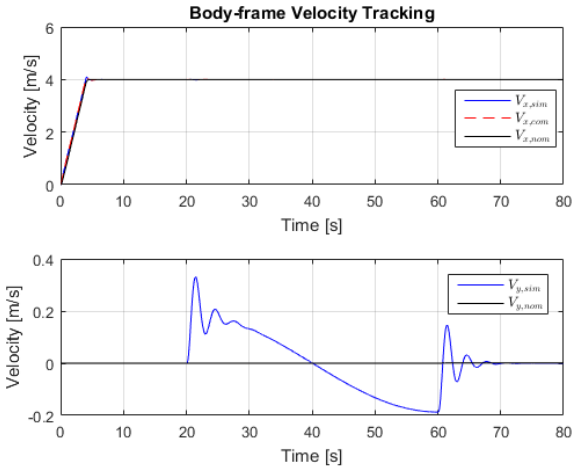

Figure 11: Velocity Tracking in b-frame

[5] Normey-Rico, Julio E.,et al. Camacho. "A Smith-predictor-based generalised predictive controller for mobile robot path-tracking." Control Engineering Practice 7.6 (1999): 729-740.

[6] Raffo, Guilherme V., et al. "A predictive controller for autonomous vehicle path tracking." IEEE Trans on intelligent transportation systems 10.1 (2009): 92-102.

[7] Weiskircher, Thomas, and Beshah Ayalew. "Predictive trajectory guidance for (semi-) autonomous vehicles in public traffic." American Control Conference. IEEE, 2015.

[8] Gao, Yiqi. Model Predictive Control for Autonomous and Semiautonomous Vehicles. Diss. University of California, Berkeley, 2014.

[9] Garcia, Carlos E., David M. Prett, et al. "Model predictive control: theory and practicea survey." Automatica 25.3 (1989): 335-348.

[10] Morari, Manfred, et al. "Model predictive control: past, present and future." Computers & Chemical Engineering 23.4 (1999): 667-682.

[11] Snider, Jarrod M. "Automatic steering methods for autonomous automobile path tracking." Robotics Institute, Pittsburgh, PA, Tech. Rep. CMU-RITR-09-08 (2009).

[12] Aguilar, Luis E., et al. "Robust path following control for wheeled robots via sliding mode techniques." Intelligent Robots and Systems, Proceedings of the IEEE/RSJ International Conference on. Vol. 3. IEEE, 1997.

[13] Paden, Brian, et al. "A Survey of Motion Planning and Control Techniques for Self-driving Urban Vehicles." IEEE

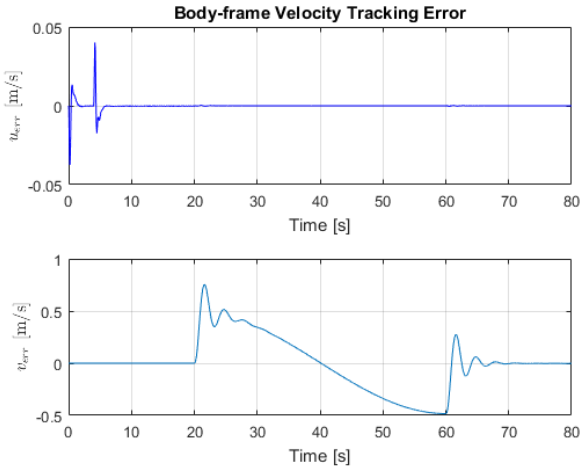

Figure 12: Velocity Tracking in b-frame

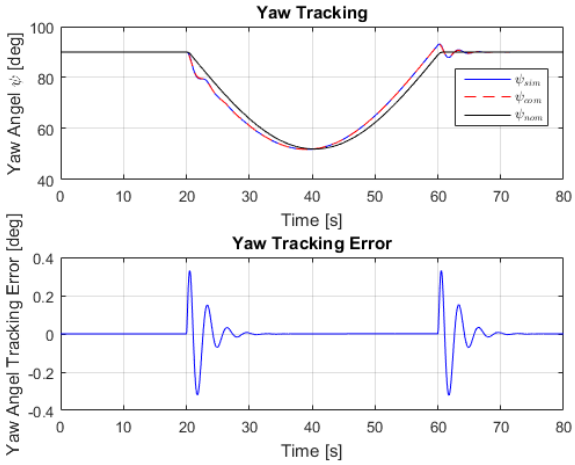

Figure 13: Yaw Angle Tracking

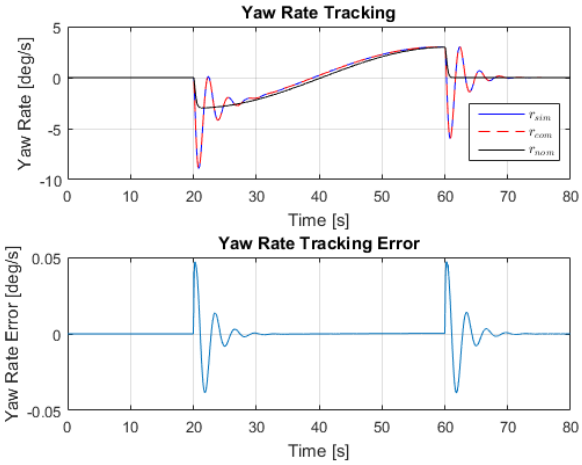

Figure 14: Yaw rate tracking

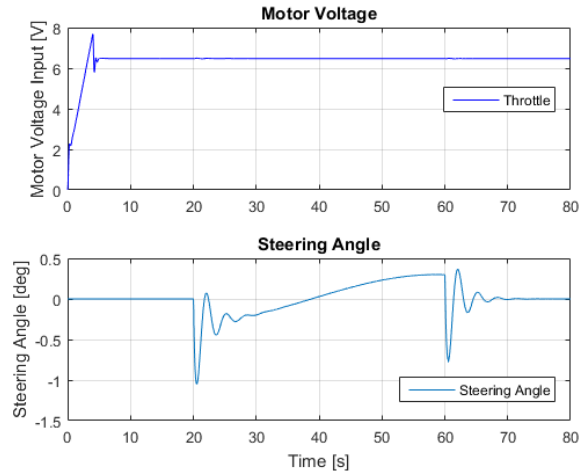

Figure 15: Actuator Signal

Trans on Intelligent Vehicles 1.1 (2016): 33-55.

[14] Aguiar, A. Pedro, and Joao P. Hespanha. "Trajectory-tracking and path-following of underactuated autonomous vehicles with parametric modeling uncertainty." IEEE Trans on Automatic Control 52.8 (2007): 1362-1379.

[15] Kanayama, Yutaka, et al. "A stable tracking control method for an autonomous mobile robot." IEEE International Conference on Robotics and Automation. IEEE, 1990.

[16] d'Andra-Novel, Brigitte, et al. "Control of nonholonomic wheeled mobile robots by state feedback linearization." The International journal of robotics research 14.6 (1995): 543-559.

[17] Huang, Rui, et al. "Guidance, navigation and control system design for a tri-propeller VTOL UAV." AIAA Guidance, Navigation and Control Conference and Exhibit, Hilton Head, South Carolina. 2007.

[18] Adami, Tony M., and J. Jim Zhu. "6DOF flight control of fixed-wing aircraft by trajectory linearization." Proceedings of the American Control Conference. IEEE, 2011.

[19] Liu, Yong, et al. "Omni-directional mobile robot controller based on trajectory linearization." Robotics and Autonomous Systems 56.5 (2008): 461-479.

[20] Zhao, Yue, and J. Jim Zhu. "Aircraft loss-of-control arrest autopilot using trajectory linearization control." 2016 American Control Conference (ACC). IEEE, 2016.

[21] Rajamani, Rajesh. Vehicle dynamics and control. Springer Science & Business Media, 2011.